Highly Disordered Crystal Structure and Thermoelectric Properties of Sn_3P_4

Julia V. Zaikina,[†] Kirill A. Kovnir,[‡,§] Alexey N. Sobolev,[†] Igor A. Presniakov,[†] Vladimir G. Kytin,[||] Vladimir A. Kulbachinskii,[||] Andrei V. Olenev,[†,⊥] Oleg I. Lebedev,[⊥] Gustaaf Van Tendeloo,[⊥] Evgeny V. Dikarev,[#] and Andrei V. Shevelkov*[,†]

Departments of Chemistry, Materials Sciences, and Physics, Lomonosov Moscow State University, Moscow 119991, Russia, Electron Microscopy for Materials Science, University of Antwerp, B-2020 Antwerp, Belgium, and Department of Chemistry, University at Albany, Albany, New York 12222

Received September 17, 2007. Revised Manuscript Received January 18, 2008

The crystal structure of Sn_3P_4, a long-known tin phosphide, has been determined. It crystallizes in the trigonal space group $R\bar{3}m$ with unit-cell parameters $a = 4.4315(1)$ Å and $c = 28.393(1)$ Å ($Z = 3$). The crystal structure of Sn_3P_4 is disordered. It consists of alternating layers of phosphorus and tin atoms that are combined into five-layer blocks and propagate along the *c*-axis. The major structural feature is the disordered orientation of the P_2^{4-} dumbbells, which link the tin atoms. The latter possess two types of coordination. One third of the tin atoms reside inside the block and are octahedrally coordinated by phosphorus atoms. The rest of the tin atoms confine the block and possess a [3 + 3] environment made up of three close phosphorus neighbors and three rather distant (3.4 Å) tin atoms of the adjacent block. The coordination of the tin atoms is confirmed by ^{119}Sn Mössbauer spectroscopy. The electron diffraction and high-resolution electron microscopy data reveal ordered regions at the microscopic level, which do not result in any superstructure formation for the bulk sample. Physical property measurements show that Sn_3P_4 is a narrow-gap semiconductor. Upon cooling to 150 K it undergoes a remarkable transition from *n*-type conduction with electrons as charge carriers to *p*-type conduction with holes as charge carries. Despite the large amount of disorder in the crystal structure, Sn_3P_4 has a relatively high thermal conductivity of about 8 W m^{-1} K^{-1}.

Introduction

Disordered narrow-gap semiconductors have recently been investigated in the context of a search for new thermoelectric materials. The discovery of a rather high thermoelectric performance for the structurally disordered β-Zn_4Sb_3 and the absence of the latter property for the fully ordered α-Zn_4Sb_3 suggest that the order–disorder phenomenon plays an important role in the formation of efficient thermoelectric materials.[1] The efficiency of a thermoelectric is expressed by its dimensionless figure-of-merit $ZT = S^2T\sigma/\kappa$, which indicates that a good thermoelectric should combine high values of the Seebeck coefficient (S), and high electrical conductivity (σ), with low thermal conductivity (κ). It is proposed that the low thermal conductivity of β-Zn_4Sb_3 originates from the structural disorder, the true nature of which is, however, not clear yet. The literature data show that ternary and even more complex compounds with a high degree of disorder and perspective values of the thermoelectric figure-of-merit due to low thermal conductivity also exist.[2]

In our recent research, we came across a tin phosphide, Sn_3P_4. It is one of four known binary tin phosphides along with Sn_4P_3,[3,4] SnP,[5] and SnP_3.[6] The crystal structure of Sn_3P_4 long remained unsolved since its discovery by Vivian in

* To whom correspondence should be addressed. Fax: +7-495-939-4788. E-mail: shev@inorg.chem.msu.ru.
† Department of Chemistry, Lomonosov Moscow State University.
‡ Department of Materials Sciences, Lomonosov Moscow State University.
§ Present address: Max-Planck-Institute for Chemical Physics of Solids, 01187 Dresden, Germany.
|| Department of Physics, Lomonosov Moscow State University.
⊥ Electron Microscopy for Materials Science, University of Antwerp.
Department of Chemistry, University at Albany.

(1) (a) Caillat, T.; Fleurial, J.; Borshchevsky, A. *J. Phys. Chem. Solids* **1997**, *58*, 1119–1125. (b) Ueno, K.; Yamamoto, A.; Noguchi, T.; Inoue, T.; Sodeoka, S.; Takazawa, H.; Lee, C. H.; Obara, H. *J. Alloys Compd.* **2004**, *384*, 254–260. (c) Nylén, J.; Andersson, M.; Lidin, S.; Häussermann, U. *J. Am. Chem. Soc.* **2004**, *126*, 16306–16307. (d) Mikhaylushkin, A. S.; Nylén, J.; Häussermann, U. *Chem.—Eur. J.* **2005**, *11*, 4912–4920. (e) Ueno, K.; Yamamoto, A.; Noguchi, T.; Li, C. H.; Inoue, T.; Sodeoka, S.; Obara, H. *J. Alloys Compd.* **2006**, *417*, 259–263. (f) Hermann, R. P.; Grandjean, F.; Chen, T. C.; Brown, D. E.; Johnson, C. E.; Snyder, G. J.; Long, G. J. *Inorg. Chem.* **2007**, *46*, 767–770.

(2) (a) Hsu, K. F.; Loo, S.; Guo, F.; Chen, W.; Dyck, J. S.; Uher, C.; Hogan, T.; Polychroniadis, E. K.; Kanatzidis, M. G. *Science* **2004**, *303*, 818–821. (b) Karkamkar, A. J.; Kanatzidis, M. G. *J. Am. Chem. Soc.* **2006**, *128*, 6002–6003. (c) Cuia, J. L.; Xueb, H. F.; Xiub, W. J.; Jiang, L.; Ying, P. Z. *J. Solid State Chem.* **2006**, *179*, 3751–3755. (d) Poudeu, P. F. P.; Angelo, J. D.; Downey, A. D.; Short, J. L.; Hogan, T. P.; Kanatzidis, M. G. *Angew. Chem., Int. Ed.* **2006**, *45*, 3835–3839. (e) Zaikina, J. V.; Kovnir, K. A.; Sobolev, A. V.; Presniakov, I. A.; Prots, Yu.; Baitinger, M.; Schnelle, W.; Olenev, A. V.; Lebedev, O. I.; Van Tendeloo, G.; Grin, Yu.; Shevelkov, A. V. *Chem.—Eur. J.* **2007**, *13*, 5090–5099.

(3) (a) Olofsson, O. *Acta Chem. Scand.* **1970**, *24*, 1153–1162. (b) Häggström, L.; Gullman, J.; Ericsson, T.; Wäppling, R. *J. Solid State Chem.* **1975**, *13*, 204–207.

(4) (a) Eckerlin, P.; Kischio, W. *Z. Anorg. Allg. Chem.* **1968**, *363*, 1–9. (b) Kuz'ma, Yu. B.; Chikhrii, S. I.; Davydov, V. N. *Neorg. Mater* **1999**, *35*, 17–18.

(5) (a) Katz, G.; Kohn, J. A.; Broder, J. D. *Acta Crystallogr.* **1957**, *10*, 607–607. (b) Donohue, P. C. *Inorg. Chem.* **1970**, *9*, 335–337. (c) Gulman, J. *J. Solid State Chem.* **1990**, *87*, 202–207.

(6) Gullman, J.; Olofsson, O. *J. Solid State Chem.* **1972**, *5*, 441–445.

10.1021/cm702655g CCC: $40.75
Published on Web 03/07/2008

1920.[7] Huang and Feng[8] have used first-principle pseudopotential calculations to suggest a pseudocubic structure corresponding to the defect zinc blende structure as the most stable one for Sn_3P_4. This, however, contradicts the X-ray powder data by Olofsson,[3a] suggesting rhombohedral symmetry. In this work, we describe the highly disordered crystal structure of Sn_3P_4 determined by a combination of X-ray single crystal diffraction, electron diffraction, and ^{119}Sn Mössbauer spectroscopy, and compare it with the closely related crystal structures of Sn_4P_3 and SnP. We also report on the thermoelectric properties of the title compound and discuss them in light of their structure–property relationship.

Experimental Section

Sample Preparation. All manipulations were carried out in an argon-filled glovebox (content of $O_2 < 1.2$ ppm, $H_2O < 1$ ppm). Fine-dispersed powders of metallic tin (Chempur, 99.99%) and red phosphorus (Chempur, 99.995%) were used as received. The preparation of tin phosphide, Sn_3P_4, generally followed the procedure described in the literature.[3b] Phosphorus was first mechanically reground in an agate mortar and then was mixed with tin in a molar ratio of 3:4 (total weight 0.5 g). The obtained powder was pressed into a pellet, sealed in a silica tube under vacuum, and then annealed at 735 K for 7 days followed by quenching the ampule in water.

Single crystals of Sn_3P_4 suitable for X-ray structure determination were selected from the reaction product of a mixture of tin, phosphorus and tin chloride $SnCl_2$ (Alfa Aesar, 99.99%) in a molar ratio of Sn:P:Cl = 4:3:1 that was annealed at 725 K for 5 days. Other crystals for X-ray structural determination were obtained by slow cooling (0.1 K/min) of the preliminary synthesized Sn_3P_4 sample after it was heated to 875 K.

Sample Characterization. The samples were characterized by means of X-ray powder diffraction (XRD). The X-ray analysis was performed using a Huber G670 Image Plate Camera, Cu $K\alpha_1$ radiation, $\lambda = 1.540598$ Å; the unit-cell parameters were calculated from least-squares fits using LaB_6 (cubic, $a = 4.15692$ Å) as an internal standard utilizing the program package WinCSD.[9] To check for the presence of superstructure reflections in the X-ray powder pattern of the annealed bulk sample of Sn_3P_4 and to perform Rietveld refinement, X-ray powder diffraction data were collected using the STOE-STADI P diffractometer (linear PSD; Cu $K\alpha_1$ radiation; $8° \leq 2\theta \leq 105°$, step width 0.01°, acquisition time 34.8 s/point. Rietveld refinement was executed with JANA2000 program package.[10]

Single-Crystal X-ray Diffraction. A suitable single crystal of Sn_3P_4 obtained by annealing tin, phoshorus, and tin(II) chloride was glued with epoxy cement on the tip of a Pyrex fiber and mounted on a goniometer head of a CAD-4 (Nonius) diffractometer. The orientation matrix was refined on the basis of 24 well-centered reflections in the angular range of $15° < \theta < 17°$ and the derived lattice parameters agreed fairly well with those found from the powder data for the bulk sample. X-ray data were recorded at room temperature and corrected for polarization and Lorentz effects. A semiempirical absorption correction was applied based on azimuthal scans of five reflections having χ angles close to 90°. The details of the crystal structure determination using SHELX programs[11] are described in the "Results and Discussion" section.

Several crystals obtained by different methods (see Sample Preparation) were additionally tested at 173 K using a Bruker SMART APEX CCD-based X-ray diffractometer system equipped with a Mo-target X-ray tube ($\lambda = 0.71073$ Å) operated at 1800 W power.

Electron Diffraction and EDX Analysis. Electron diffraction (ED) patterns and EDX analysis were carried out on a CM20 Philips microscope with the LINK 2000 analytical attachment. High-resolution electron microscopy (HREM) investigations were performed using a JEOL 4000 EX microscope operating at 400 kV. The sample for TEM was crushed, dispersed in methanol, and deposited on a holey carbon grid. Simulation of the HREM images was performed using the Mac Tempas and Crystal Kit software.

Differential Scanning Calorimetry (DSC). DSC investigation was performed with the Netzsch DSC 409c equipment in a sealed under vacuum quartz glass crucible in the temperature range of 300–973 K with a heating rate of 5 K/min (sample mass 144.5 mg). After cooling with the same rate, the sample was examined by powder XRD.

Mössbauer Spectroscopy. The ^{119}Sn spectrum was recorded using a conventional constant acceleration Mössbauer spectrometer. The measurements were performed at 300 K with the $Ca^{119m}SnO_3$ source maintained at room temperature. Isomer chemical shifts are referenced to the $CaSnO_3$ absorber at 300 K.

Physical Property Measurements. For the property measurements, a sample of Sn_3P_4 was hot-presses at 573 K in a WC press die under argon. Afterward, a parallelepiped bar of approximately $1 \times 1 \times 5$ mm was cut from the dense pellet. To check the possibility of decomposition, an XRD analysis of the sample after the hot pressing was performed, and no changes in X-ray pattern were detected.

The simultaneous measurements of the Seebeck coefficient, thermal conductivity, and electrical resistivity were performed using a precalibrated original experimental setup including a low temperature cryostat. Measurements of all quantities have been made by the four-probe method. The sample chamber was evacuated up to 1×10^{-5} mbar. Temperature was controlled by the main heater and measured by a calibrated carbon resistance thermometer TSU-2. Another heater was used to apply small temperature gradient (0–1 K) to the sample. The temperature gradient has been measured by a Cu/Cu−Fe thermocouple. Potentials on the sample and on the Cu/Cu−Fe thermocouple have been measured by R3003 voltmeters.

The Hall effect has been measured at the setup consisting of an electromagnet producing a magnetic field up to 0.7 T. Stabilized current was applied to the sample. Hall measurements were performed at room temperature (293 K) and in liquid nitrogen (77 K).

Results and Discussion

Synthesis, X-ray Powder Data, and EDX Analysis. We have attempted several synthesis conditions for the preparation of Sn_3P_4 in the form of a pure phase. We tried various temperatures and durations of annealing, quenching or slow cooling, pressing of starting material into pellets, using tin iodide(IV) as transport agent as well as lead chloride or lead as fluxes. The best conditions were found to be those that

(7) Vivian, A. C. *J. Inst. Met.* **1920**, *23*, 325–336.
(8) Huang, M.; Feng, Y. P. *Phys. Rev. B* **2004**, *70*, 184116(1–5).
(9) Akselrud, L. G.; Zavalij, P. Y.; Grin, Yu. N.; Pecharsky, V. K.; Baumgarthner, B.; Wölfel, E. *Mater. Sci. Forum* **1993**, *133–136*, 335–337.
(10) Petricek, V.; Dusek, M.; Palatinus, L. *JANA 2000*; Institute of Physics, Academy of Science of the Czech Republic: Prague, Czech Republic, 2002.
(11) (a) Sheldrik, G. M. *SHELXS-97, Program for Crystal Structure Solution*; University of Göttingen: Göttingen, Germany, 1997. (b) Sheldrik, G. M. *SHELXL-97, Program for Crystal Structure Refinement*; University of Göttingen: Göttingen, Germany, 1997.

generally follow the synthetic procedure described in the literature;[3b] however, even under these optimal conditions, the product contained detectable amounts of Sn_4P_3 as well as no single crystals suitable for X-ray structural investigation.

X-ray powder analysis of this sample showed the presence of the tin phosphide, Sn_3P_4, along with the Sn_4P_3 impurity. In addition, traces of white phosphorus deposited on the ampule walls were clearly observed. The diffraction pattern, excluding the peaks belonging to Sn_4P_3, was completely indexed in a trigonal *R*-centered system with unit-cell parameters $a = 4.4315(1)$ Å and $c = 28.393(1)$ Å. These parameters were obtained from least-squares fits of the positions of the diffraction maxima using LaB_6 as an internal standard and did not change within the accuracy of determination for several different samples. The unit-cell parameters and symmetry agree well with the literature data.[3] To estimate the relative amount of impurity of another tin phosphide, Sn_4P_3, in the sample, we performed a Rietveld analysis. Structural data for the initial model were taken from the single-crystal experiments (see below) as well as from the literature data for Sn_4P_3.[4b] The amount of the target phase Sn_3P_4 was found to be approximately 90 mass %. The Sn:P ratio of the Sn_3P_4 phase investigated by the EDX analysis was found to be 43(1):56(1), which is in a good agreement with that calculated for Sn_3P_4, 42.9:57.1.

Investigation of the homogeneity range of Sn_3P_4 is hampered by the presence of phosphorus vapor in the ampoules. We performed the synthesis (same conditions, see Experimental Section) of the two samples with the nominal compositions $Sn_{39}P_{61}$ and $Sn_{46}P_{54}$, which should lie in the two-phase regions around Sn_3P_4 ($Sn_{43}P_{57}$) according to the reported phase diagram.[12] The unit-cell parameters for the two samples were refined using the sets of the same reflections with LaB_6 as an internal standard: $Sn_{39}P_{61}$, $a = 4.4306(2)$ Å, $c = 28.386(2)$ Å; $Sn_{46}P_{54}$, $a = 4.4312(1)$ Å, $c = 28.397(1)$ Å. The difference in unit-cell parameters is quite small, indicating a very narrow homogeneity range for Sn_3P_4.

The DSC investigation shows that during the heating of a Sn_3P_4 sample a strong endothermic peak appears at ~830 K, which is close to melting temperature reported in the literature.[7,12] After cooling down, the large amount of red phosphorus was clearly observed on the ampule walls in the upper part of the ampule, which probably was transported thorough the gas phase. XRD shows that the sample after DSC experiment consists mainly of Sn_4P_3 (~70%), while Sn_3P_4 is present as a minor phase (~30%). The unit-cell parameters of Sn_3P_4 before and after the DSC experiment were the same within one standard deviation. The presence of a large amount of red phosphorus and Sn_4P_3 contradicts with the phase diagram[12] where congruent melting at 833 K is given for Sn_3P_4. Apparently, in phase diagram studies, the presence of the gas phase and its influence on the phase equilibrium in the Sn–P system was not taken into account. From our DSC investigation, we can conclude that at a temperature of 830 K and a pressure lower than 1×10^{-3} mbar Sn_3P_4 decomposes into phosphorus and a tin-rich phosphide, Sn_4P_3.

$$4Sn_3P_4 \rightarrow 3Sn_4P_3 + 7P$$

According to the Sn–P phase diagram,[12] Sn_3P_4 has a wide homogeneity range (2 at. % at the synthesis temperature of 735 K) and melts congruently at 833 K. The analysis of the literature provides the evidence that this part of the Sn−P phase diagram is based on the earlier (1920) work of Vivian.[7] Our data, both synthetic and DSC, contradict with the reported phase diagram in the following. First, it was not possible to synthesized Sn_3P_4 by slow cooling of the stoichiometric composition from temperatures higher than 833 K; second, no considerable phase range was detected. Indeed, all Sn_3P_4 samples prepared in different ways, by annealing of the elements, by transport reaction with SnI_4, $SnCl_2$, or $PbCl_2$, or by flux synthesis, have the same unit cell parameters within 3 esd (estimated standard deviation). It should be noted here that a significant homogeneity range was also reported for another tin phosphide Sn_4P_3,[4a] whereas our recent results show that Sn_4P_3 has a very narrow homogeneity range, if any.[13] The discrepancy of observed and reported homogeneity range of Sn_3P_4 may be explained by the existence of another tin phosphide SnP,[5c] having a hexagonal ambient pressure modification with a similar *a* unit-cell parameter (Sn_3P_4, 4.4315 Å; SnP, 4.3922 Å). SnP (50 at.% phosphorus) is not considered on the tin−phosphorus phase diagram,[12] but it should lie between Sn_4P_3 (43 at % phosphorus) and Sn_3P_4 (57 at % phosphorus). Though the hexagonal SnP is considered as an ambient-pressure modification, it is not present on the Sn–P phase diagram and its synthesis requires a certain pressure of phosphorus in an ampule.[5c]

The single crystal of Sn_3P_4 used for X-ray structure determination was found in the reaction product after annealing the powder mixture of tin, phosphorus, and tin(II) chloride. According to the X-ray powder data the sample contained the target Sn_3P_4 phase along with another tin phosphide, Sn_4P_3, tin(II) chloride, and traces of white phosphorus.

Crystal Structure Determination and Description. The structure of tin phosphide, Sn_3P_4, was determined by single-crystal X-ray diffraction methods at ambient temperature. The data set was indexed in the hexagonal unit cell with parameters $a = 4.4290(6)$ Å and $c = 28.360(6)$ Å, which is in a good agreement with the powder diffraction data. No additional systematic extinctions, except those corresponding to the *R*-centered trigonal lattice [*hkl*], $-h + k + l = 3n$, were observed. Examination of systematic absences in the X-ray single-crystal data set suggests the possible space groups *R*3, $R\bar{3}$, *R*32, *R*3*m*, and $R\bar{3}m$. The $R\bar{3}m$ (No. 166) group of the highest symmetry was chosen for the structure solution ($R_{int} = 0.048$). The positions of two tin atoms, Sn(1) and Sn(2), were obtained from direct methods (SHELXS[11a]). Four phosphorus atoms were located from a combination of least-squares refinement and difference Fourier maps (SHELXL[11b]). Further refinement showed that phosphorus

(12) Massalski, Th. B., Okamoto, H., Subramian, P. R., Kacprzak, L., Eds. *Binary Alloy Phase Diagrams*, 2nd ed.; ASM International: Materials Park, OH, 1996.

(13) Kovnir, K. A.; Kolen'ko, Yu. V.; Ray, S.; Li, J.; Watanabe, T.; Itoh, M.; Yoshimura, M.; Shevelkov, A. V. *J. Solid State Chem.* **2006**, *179*, 3756–3762.

Table 1. Data Collection and Structure Refinement Parameters for Sn_3P_4

composition	$Sn_3P_{4.03(7)}$
cryst syst	trigonal
space group	$R\bar{3}m$, No. 166
data collection temperature (K)	293(2)
cell params (Å)	$a = 4.4290(6)$, $c = 28.360(6)$
V (Å^3)	481.8(1)
Z	3
λ (Å)	Mo Kα, 0.71073
density (calcd) (g cm^{-3})	4.963
μ (mm^{-1})	12.44
no. of reflns collected	1430
no. of independent reflns	289 [$R_{int} = 0.0483$]
no. of params refined	29
R_1	0.023
wR_2 [$F_o > 4\sigma F_o$]	0.057
largest diff. peak and hole (e/Å^3)	2.43 and –0.91
GOF	1.168

Table 2. Atomic Coordinates, Site Occupancy Factors (s.o.f.), and Equivalent Displacement Parameters for Sn_3P_4

atom	position	*x*/*a*	*y*/*b*	*z*/*c*	s.o.f.	U_{eq}[a]
Sn(1)	3*a*	0	0	0	1	0.0102(1)
Sn(2)	6*c*	0	0	0.79447(1)	1	0.0135(1)
P(1)	6*c*	0	0	0.4330(2)	0.24(1)	0.009(1)
P(2)	6*c*	0	0	0.3574(1)	0.222(9)	0.006(1)
P(3)	18*h*	0.2043(4)	–*x*	0.0771(1)	0.261(4)	0.0117(7)
P(4)	18*h*	0.1385(7)	–*x*	0.3861(1)	0.256(4)	0.0100(7)

[a] U_{eq} is defined as one-third of the trace of the orthogonalized U_{ij} tensor.

Table 3. Interatomic Distances in the Structure of Sn_3P_4

bond	distance (Å)
Sn(1)–P(2)	2.647(2)
Sn(1)–P(3)	2.690(3)
Sn(1)–P(4)	2.681(2)
Sn(2)–Sn(2)	3.3762(6)
Sn(2)–P(1)	2.678(2)
Sn(2)–P(3)	2.656(2)
Sn(2)–P(4)	2.600(2)
P(1)–P(2)	2.145(9)
P(3)–P(4)	2.166(5)

atoms have short (physically impossible) distances to each other as well as large atomic displacement parameters. Therefore, the occupancy factors for phosphorus were refined independently and found to be approximately ¼ for each of the four positions. The occupancy factors for tin atoms turned out to be equal to unity. The final refinement with anisotropic atomic displacement parameters for all atoms converged to $R = 0.023$ leading to the composition $Sn_3P_{4.03(7)}$. Refinement in other possible space groups ($R3$, $R\bar{3}$, $R32$, $R3m$) led to higher R-values and did not remove the disorder of phosphorus positions. The experimental parameters are listed in Table 1; the atomic parameters are given in Table 2; and interatomic distances are presented in Table 3.

Crystals of Sn_3P_4 obtained by two different methods (see Sample Preparation) and tested on CAD-4 and SMART-APEX CCD diffractometers all exhibited the same symmetry and unit-cell parameters, with no additional reflections corresponding to a possible superstructure. However, all these crystals were found to be of the poorer quality or were complicated twins.

The structure of Sn_3P_4 (Figure 1, left) consists of alternating layers of phosphorus and tin atoms that are combined into five-layer blocks that propagate along the *c*-axis. There

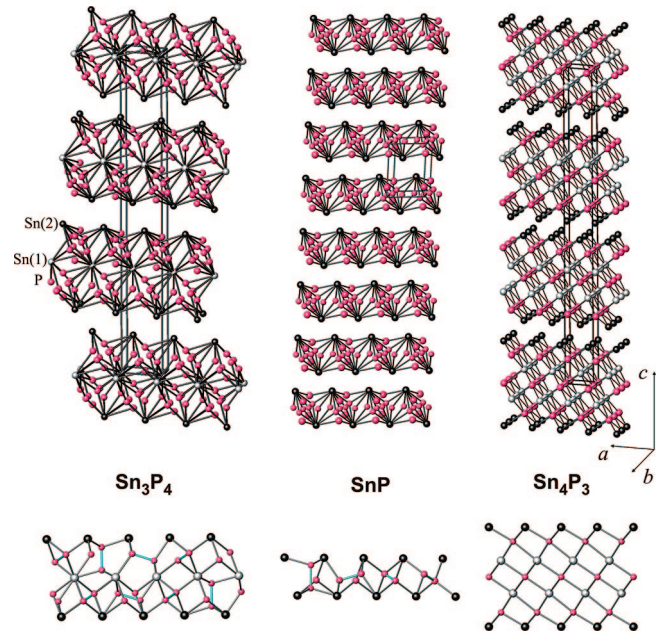

Figure 1. General view of the crystal structures (top) and [10–10] projection of one layer (bottom) of Sn_3P_4 (left), SnP (middle), and Sn_4P_3 (right). Sn(1), gray circles; Sn(2), black circles; phosphorus atoms, pink circles, P–P bonds shown in cyan. For the Sn_3P_4 and SnP structures, all statistically possible atoms are drawn for the general view (top), whereas only one variant of statistically ordered model is shown for the [10–10] projection of the layer (bottom) emphasizing four possible orientation of P_2 dumbbells.

are two types of tin atoms in the crystal structure. The Sn(1) atoms are octahedrally coordinated by phosphorus atoms only and do not form any Sn−Sn bonds. The Sn(2) atoms confining the block have a [3 + 3] coordination composed by three phosphorus atoms from one side and three Sn(2) atoms from the adjacent block at a relatively long distance of 3.38 Å. Within each block, there are one layer of Sn(1) and two layers of Sn(2), thus the Sn(1):Sn(2) ratio is 1:2. Layers of phosphorus atoms separate the layers of the tin atoms. Phosphorus atoms are disordered, but in a very special way. The P(1) and P(2) atoms are joined into pairs at a distance of 2.15 Å.[14] The P(1)−P(2) dumbbells are oriented along the *c*-axis, connecting the tin layers such that P(1) is surrounded by three Sn(2) at 2.68 Å, while P(2) is coordinated by three Sn(1) at 2.65 Å (Figure 2). The occupancy factors of the P(1) and P(2) atoms are close to ¼; therefore, only one of four P(1)–P(2) dumbbells is present. The P(3) atom is bonded to P(4) at a distance of 2.17 Å.[14] Three orientations of the P(3)−P(4) dumbbells are statistically possible, all of them are shifted from the *ab*-plane and differed from each other only by a 60° rotation. The P(3)−P(4) dumbbells also connect tin layers, but in such a way that the P(3) atom is located closer to the Sn(2) layer, forming two bonds with Sn(2) and only one bond with Sn(1), whereas the P(4) atom is coordinated by two Sn(1) and one Sn(2) atoms, being close to the Sn(1) layer (Figure 2). In all cases, the Sn−P distances cover the range of 2.60–2.69 Å, that is comparable with the corresponding distances of 2.66 Å found in SnP_3[6] and Sn_4P_3.[4b] Taking into account the occupancy

(14) The value is compatible with a single P–P bond. See: von Schnering, H. G.; Hönle, W. *Chem. Rev.* **1988**, *88*, 243–273.

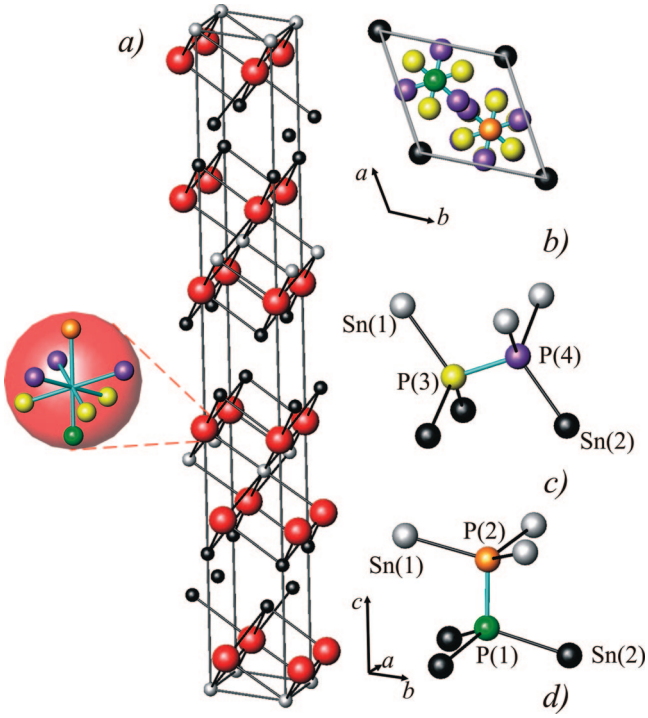

Figure 2. View of the crystal structure of Sn_3P_4: (a) a view of the unit cell showing the alternation of the tin atoms and disordered dumbbells; (b) a projection onto [0001]; environment of the (c) P(3)–P(4) and (d) P(1)–P(2) dumbbells. Sn(1), gray circles; Sn(2), black circles; P(1), green circles; P(2), orange circles; P(3), yellow circles; P(4), violet circles; P–P bonds shown in cyan; disordered dumbbells shown as large red circles.

factors for all phosphorus atoms it should be concluded that only one of four dumbbells is randomly present.

The crystal structure of Sn_3P_4 is closely related to the structure of another, more Sn-rich phosphide Sn_4P_3, (Figure 1, right), while having several important differences. The structure of Sn_4P_3 is also layered with alternating phosphorus and tin layers being grouped into seven-layer blocks. Similar to Sn_3P_4, in the crystal structure of Sn_4P_3 there are two types of tin atoms: Sn(1) is octahedrally coordinated by phosphorus atoms, while Sn(2) has a [3 + 3] coordination of three phosphorus and three tin atoms at a distance of 3.25 Å, which is shorter than the Sn(2)−Sn(2) contacts in Sn_3P_4. In the structure of Sn_4P_3, two types of tin atoms are found in equal ratio, since one tin layer is added to the block compared to the structure of Sn_3P_4. Additionally, in Sn_4P_3, all phosphorus atoms display almost 100% occupancy; they are octahedrally coordinated by only tin atoms and do not form any homonuclear bonds.

An even more striking similarity is observed between the structures of Sn_3P_4 and SnP. The latter compound has an ambient-pressure form,[5c] which possesses a disordered crystal structure built of layers of alternating tin and phosphorus atoms that are joined into blocks three layers thick (Figure 1, middle). In this structure, all phosphorus atoms form P_2^{4-} dumbbells similar to the structure of Sn_3P_4, while all tin atoms confine blocks and possess a [3 + 3] coordination like the Sn(2) atoms in Sn_3P_4 and Sn_4P_3.

To estimate the properties of Sn_3P_4, formal charges for all atoms, which stem from the atoms coordination, should be considered. The Sn(1) atoms, coordinated by six phosphorus atoms, can be regarded as Sn^{4+}. Assuming layered

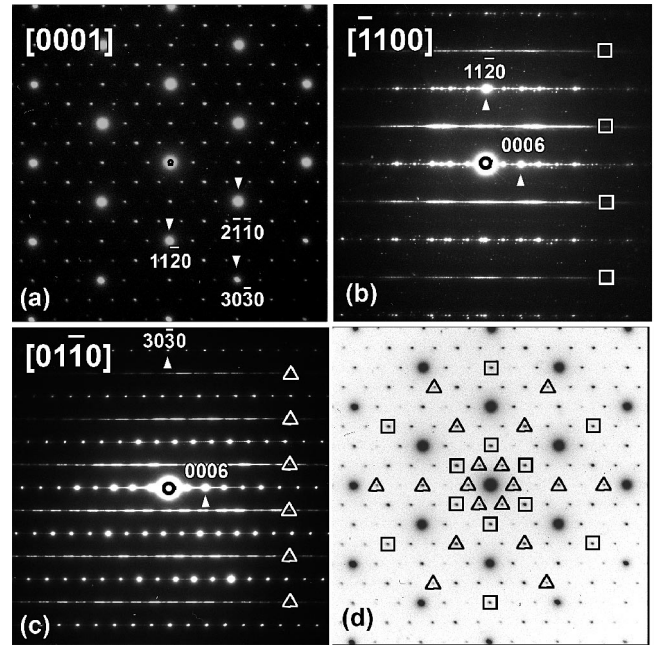

Figure 3. Electron diffraction patterns along the major zones of Sn_3P_4. See text for explanations.

character of the investigated phosphide, the Sn(2) atoms confining blocks and having only three nearest phosphorus neighbors is more close to Sn^{2+}, analogous to the tin atoms in the $SnCl_3^-$ anion.[15] Further, the P_2 dumbbells with the P–P separations typical for a single bond are reckoned to have a –4 charge. Thus, the formula of Sn_3P_4 taking into account the ratio between Sn(1) and Sn(2) atoms could be written as $Sn_3P_4 = (Sn^{4+})_1(Sn^{2+})_2(P_2^{4-})_2$, indicating that all bonding and nonbonding state are filled, whereas antibonding states are vacant. Therefore, Sn_3P_4 is expected to be a semiconductor. The same expectation is true for SnP, where the P_2^{4-} dumbbells coexist with Sn^{2+} atoms leading to the formulation $(Sn^{2+})_2(P_2^{4-})_1$. The examination of the crystal structure of Sn_4P_3 does not lead to the allocation of the formal charges to all atoms, and this compound exhibits metallic type of conductivity.[4a]

Electron Diffraction and High-Resolution Transmission Electron Microscopy. To check possible superstructure formation, which could arise from the ordering of the P−P dumbbells within different layers, an investigation of the Sn_3P_4 sample by electron diffraction (ED) was performed. Electron diffraction patterns for Sn_3P_4 along the main zones are shown in Figure 3. These ED patterns reveal some remarkable features. Only the brighter spots at the ED pattern for the [0001] orientation (Figure 3a) can be indexed using the unit cell derived from X-ray single crystal data. On the patterns taken along the [−1100] and [01–10] axes (Figures 3b and c, respectively) bright streaks spreading along the c^* axis are clearly seen. Along the [0001] zone these streaks intersect the plane and produce sharp spots (Figure 3a,d). In Figure 3d, the spots originating from streaks observed for the [−1100] and [01–10] orientations are marked by squares and triangles, respectively. At first glance, the appearance

(15) (a) $CsSnCl_3$: Poulsen, F. R.; Rasmussen, S. E. *Acta Chem. Scand.* **1970**, *24*, 150–156. (b) $[Co(CO)_4]SnCl_3$: Klüfers, P. *Z. Naturforsch., B: Chem. Sci.* **1991**, *46*, 187–191.

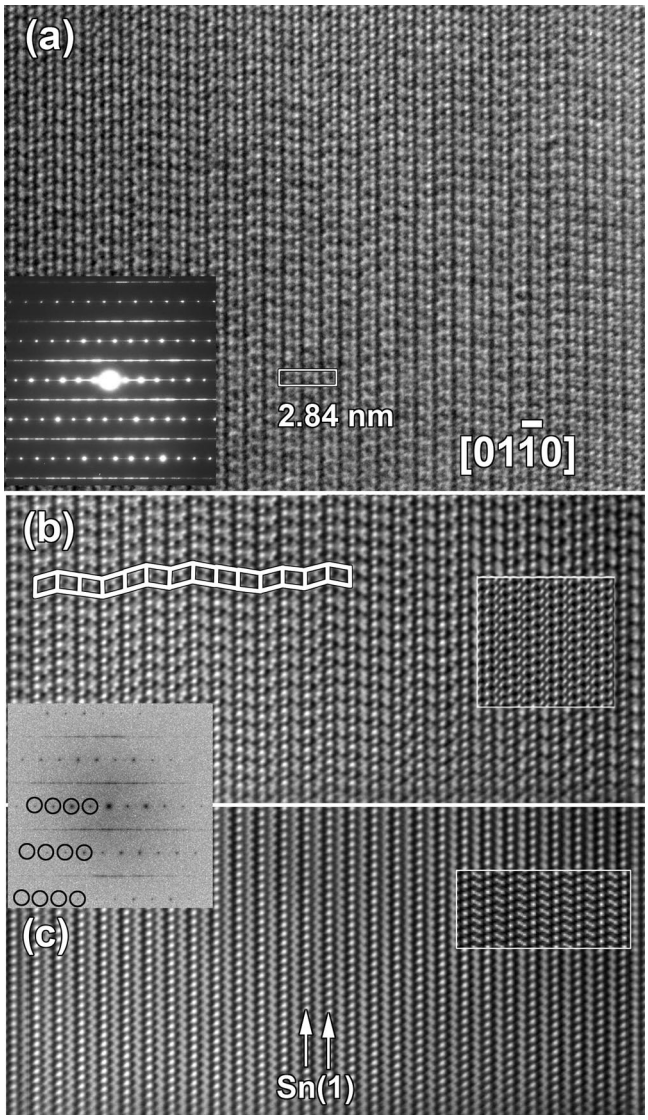

Figure 4. (a) [01–10] HRTEM image of the Sn_3P_4 and corresponding ED pattern; (b) filtered HTREM image of (a). A Bragg-mask filter was used to improve the signal-to-noise ratio. The Fourier transform (FT) is given as inset, and streaks are well observed. Tin−phosphorus blocks, stacking along the *c* axis, are marked with white quadrangles; (c) filtered HTREM image of (a). A Bragg-mask filter was used to select only the basic spots marked by cycles in the FT. A simulated image based on the X-ray data together with a proposed ordered model are given as insets in (c) and (b), correspondingly (Δf = –50 nm, t = 9 nm).

of such spots might suggest an increase of the *a* parameter of the unit cell multiplying it by $2\sqrt{3}$. Such a transformation of the unit cell, however, neither explains the nature of the streaks observed at the [0001]* pattern nor corresponds to the X-ray pattern from the powdered sample where the expected superstructure peaks are absent.

To understand the nature of the streaks, a HRTEM image along [01–10] was taken from a thin area (Figure 4a). In order to enhance the signal-to-noise ratio in the image, Fourier filtering was applied using a Bragg mask. The filter size (diameter of the separate circles) was chosen in such a way that no structural information was lost but also such that no artifacts were introduced. The similarity of the filtered (Figure 4b) and experimental HRTEM image is proof of a correct filtering procedure. Remarkably, even after the filtering, the observed image and the image calculated based

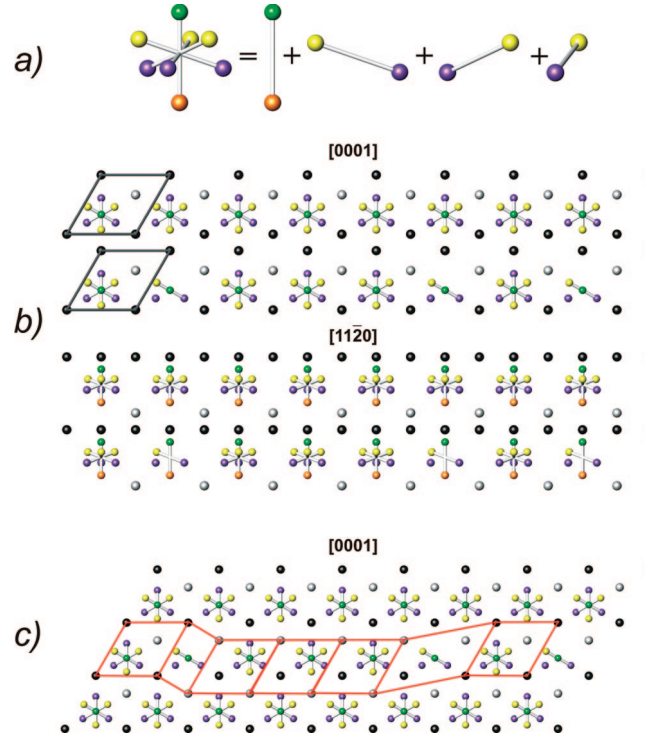

Figure 5. Structural model showing a local ordering of phosphorus atoms: (a) a disordered P_2^{4-} dumbbell as a superposition of four statistically possible dumbbells; (b) [0001] and [11–20] projections of one block of Sn_3P_4 crystal structure, fully disordered (upper layer) and partially ordered (lower layer); (c) [0001] projection of Sn_3P_4 crystal structure including partially ordered fragments. Atomic labeling corresponds to Figure 2.

on the X-ray data do not match. To reveal the nature of such discrepancy, the experimental image was carefully examined. The streaks are clearly observed, even on the Fourier transform, and the image itself has a number of peculiarities. The rows of dots are spreading along the *a* axis in such a way that a bright dot is followed by a dim dot, which can be explained by the features of the crystal structure. The refinement of the crystal structure against the X-ray data unambiguously showed that while the sites of the tin atoms are fully occupied, the phosphorus atoms, joined into dumbbells, are disordered in a way that only one out of four dumbbells can be present in each block of the structure. Consequently, the modulation of contrast, observed in Figures 4a and b, most probably corresponds to a short-range ordering of phosphorus atoms along the *a* axis. A good agreement of the observed and calculated image may be achieved introducing a partly ordered model in which disordered P_2^{4-} dumbbells alternate along *a* direction with partially ordered fragments. The disordered dumbbell is a superposition of four dumbbells with 25% occupancy each (Figure 5a). A partly ordered fragment is created such that only two of four possible dumbbells are present intact, the third is broken leaving a separate phosphorus atom, and the fourth is missing, as schematically shown in Figure 5b. When the [0001] projection is regarded, the presence of the partly ordered fragment will create a certain mismatch (as schematically shown in Figure 5c), which similar to one observed on the HREM images (shown by white lines in Figure 4b). The shift is random, which means that the disordered and partially ordered phosphorus fragments irregularly alternate

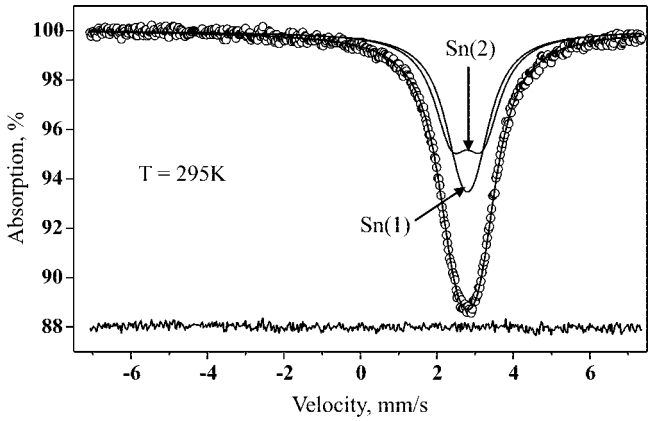

Figure 6. ^{119}Sn Mössbauer spectrum for Sn_3P_4. Straight lines show the fitting doublets.

along the *c* axis as shown in Figure 4b. This irregularity leads to the formation of streaks in the electron diffraction pattern.

The last question we would like to address is why the observed image does not match the one calculated based on the X-ray structural data? A Fourier transformation was applied to the experimental image and after that a mask was overlaid on the resulting diffraction pattern in such a way that all streaks were eliminated and only base spots, marked by circles in Figure 4b, remained. Reversed Fourier transformation resulted in the image shown in Figure 4c. As seen from the picture, a uniform intensity distribution in the rows of dots is achieved. An image calculated on the base of the X-ray structure refinement (Figure 4c, right insert) now perfectly fits in and shows that these rows of bright dots correspond to the positions of Sn(1) in the average crystal structure. Hence, the ordering of phosphorus atoms should change the coordination environment of tin leading to the alternation of differently coordinated tin atoms, which in turn leads to a modulation of the intensities in the rows spreading along the *a* direction. As the ordered phosphorus groups pack randomly along the *c* direction, the X-ray analysis performed on a relatively large crystal gives only an average structural model.

Mössbauer Spectroscopy. The Mössbauer spectrum of Sn_3P_4 shown in Figure 6 appears as a complex superposition of nonsymmetrical nonmagnetic doublets. The fitting of the spectrum was performed taking into account the high correlation of two variables, the quadrupole splitting Δ, and the line half-width $\Gamma_{1/2}$. To minimize the fitting problems, the following restrictions were imposed: the half-width for the minor component of the main subspectrum was varied within the range of 1.00–1.30 mm s^{-1}, and the hyperfine parameters for the Sn_4P_3 impurity were fixed according to the literature data.[16] This model converged (Table 4) reaching a minimum of the χ_i^2 functional at $\Gamma_{1/2} = 1.14$ mm s^{-1} for the minor component. The subsequently calculated amount of the Sn_4P_3 impurity of 8% agrees well with the X-ray phase analysis data.

The resulting doublets can be easily attributed taking into account the difference in the quadrupole splitting. One can assume that the first doublet with $\Delta = 1.36$ mm s^{-1} corresponds to the Sn(2) atom having a [3 + 3] environment made of three close phosphorus neighbors and three rather distant tin atoms. The second doublet with $\Delta = 0$ reflects an almost perfect coordination of the Sn(1) atom by six phosphorus atoms. The doublets intensity ratio is close to 2:1 as found in X-ray structure refinement for the Sn(2) and Sn(1) atoms. The close values of the chemical shifts, δ, for two components reflect a similar withdrawal of the electron density from the Sn nuclei. In particular, it shows that the Sn(2) atom should not be regarded as having a lone electron pair pointing to three distant (3.38 Å) tin neighbors. Rather, these contacts ensure bonding between the tin atoms of the adjacent blocks. A similar effect has previously been observed for several tin-containing compounds[2e,16,17] and discussed in more detail in our previous work.[17]

It should be noticed that a ^{119}Sn Mössbauer spectrum of Sn_3P_4 was recorded by Häggström et al. in 1975.[3b] The spectrum is similar to the one obtained in our work; however, the assignment of the spectrum by six overlapping singlets without knowing the crystal structure of the compound is obviously too ambiguous. At least, such an assignment neglects the number of independent tin atoms and the asymmetry of their environment.

Table 4. Hyperfine Parameters for the ^{119}Sn Mössbauer Spectrum of Sn_3P_4

position	δ (mm s^{-1})	Δ (mm s^{-1})	$\Gamma_{1/2}$ (mm s^{-1})	*S* (%)
Sn(1)	2.36(1)	0.0(1)	1.14[a]	33(1)
Sn(2)	2.46(1)	1.36(1)	0.95(1)	59(1)
Sn_4P_3	2.8[a]	0.68[a]	1.19[b]	8(1)

[a] Chosen as corresponding to the minimum of χ_i^2 (for explanation, see text). [b] Fixed according to ref 16.

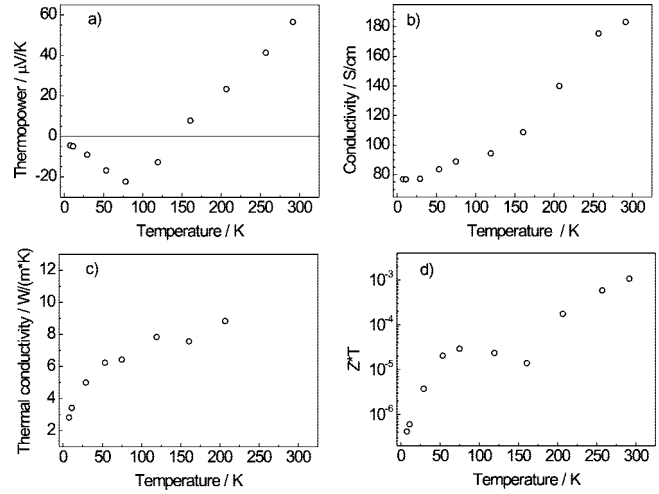

Figure 7. Thermoelectric properties of Sn_3P_4. Temperature dependences of (a) Seebeck coefficient, *S*; (b) electrical conductivity, σ; (c) thermal conductivity, κ; and (d) dimensionless figure of merit, *ZT*.

Thermoelectric Properties. The temperature dependence of Seebeck coefficient (*S*), electrical conductivity (σ), thermal conductivity (κ), and dimensionless figure of merit (*ZT*) are shown in Figure 7a–d. The absolute value of the Seebeck coefficient decreases with decreasing temperature from 55

(16) Shatruk, M. M.; Kovnir, K. A.; Lindsjö, M.; Presniakov, I. A.; Kloo, L. A.; Shevelkov, A. V. *J. Solid State Chem.* **2001**, *161*, 233–242.

(17) Kovnir, K. A.; Sobolev, A. V.; Presniakov, I. A.; Lebedev, O. I.; Van Tendeloo, G.; Schnelle, W.; Grin, Yu.; Shevelkov, A. V. *Inorg. Chem.* **2005**, *44*, 8786–8793.

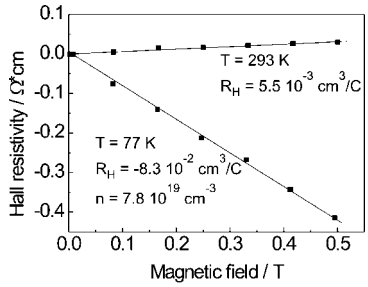

Figure 8. Magnetic field dependence of the Hall resistivity for Sn_3P_4 at 293 and 77 K.

μV K^{-1} at room temperature, then changes its sign, increases to -25 μV K^{-1} at 75 K and drops to -5 μV K^{-1} at 5 K. At $T \approx 150$ K, the Seebeck coefficient changes its sign from negative to positive with an increase of temperature, indicating a transition from dominating *n*-type conductivity to dominating *p*-type conductivity. This is also confirmed by the Hall effect measurements. The results of these measurements are shown in Figure 8. At room temperature the Hall coefficient is positive and equal to 5.5×10^{-3} cm^3 C^{-1}, whereas at 77 K it is negative and equal to -8.3×10^{-2} cm^3 C^{-1}.

Sn_3P_4 has a semiconductor-like temperature dependence of conductivity: its electrical conductivity decreases with decreasing temperature. However, this tendency saturates at low temperature and the conductivity tends to a nonzero value at temperatures close to 0 K. This indicates that at low temperatures Sn_3P_4 is a degenerate *n*-type semiconductor. The electron concentration at 77 K, calculated from the Hall effect with a Hall factor equal to unity, is 7.8×10^{19} cm^{-3}. Then, the electron mobility calculated using this concentration is 6.5 cm^2 V^{-1} s^{-1}. Such a low value of electron mobility indicates a high concentration of defects. These defects can be grain boundaries or inclusions of the Sn_4P_3 admixture. With temperature increase, the type of dominating charge carrier changes; this is confirmed by the reverse of sign of the Hall constant and is also witnessed by the inflection on the $\sigma(T)$ curve at about 150 K. Thus, at room temperature, holes contribute to the conductivity more than electrons. In the *n*-type semiconductor the holes can only be intrinsic, i.e., thermally activated from the conduction band, and their mobility is higher than the electron mobility as concluded from the positive Hall constant. Therefore, Sn_3P_4 has to be a narrow gap semiconductor. It should be noted that the admixture of Sn_4P_3, which is metallic and have a Seebeck coefficient of $+5$ μV K^{-1} at room temperature,[4a] to the title compound could not change drastically the properties of Sn_3P_4. The admixture is small enough and therefore can play only a role of the scattering centers for electrons and phonons.

The thermal conductivity κ (T) for Sn_3P_4, shown in Figure 7c, slightly increases between 0 and 50 K and then virtually does not depend on temperature up to $T = 150$ K. The value of κ at 150 K, not influenced by radiation losses and thus corresponding to the intrinsic property of the compound, is about 8 W m^{-1} K^{-1}. The thermal conductivity of a compound is determined by phonon spectrum and phonon scattering. The temperature dependence of the thermal conductivity indicates that the phonon scattering by defects is the main phonon scattering mechanism in this material. The measured value of the thermal conductivity is quite large but comparable with that of such thermoelectric materials as Sb_2Te_3. It is significantly larger than in zinc antimonide, Zn_4Sb_3,[1b] due to the larger mean group velocity of phonons, which may stem from the fact that in the latter structure three partly occupied zinc atomic positions display very large atomic displacement parameters. Relatively high thermal conductivity together with the relatively small value of the Seebeck coefficient of several tens μV K^{-1} for Sn_3P_4 leads to a low value of the thermoelectric efficiency (about 3×10^{-3} at room temperature). Most probably this is due to compensation (both electrons and holes contribute to the conductivity) at room temperature.

Conclusions

Sn_3P_4, a long-known, yet less-studied tin phosphide, has a complicated crystal structure composed of tin and phosphorus atoms grouped into blocks five layers thick. The positioning of two types of tin atoms having different coordination ensures its trigonal symmetry. These tin atoms evoke almost the same chemical shifts in the ^{119}Sn Mössbauer spectrum, which, in particular, indicates that the interaction of the tin atoms from the adjacent blocks, lying 3.4 Å apart, is bonding. Phosphorus atoms are joined into the P_2^{4-} dumbbells that have four statistically possible orientations within the block, leading to a disorder in the crystal structure. The bulk sample does not show any sign of superstructure formation, though the electron microscopy study indicates the existence of local ordered regions. According to the thermoelectric properties and Hall effect measurements, Sn_3P_4 is most probably a narrow gap semiconductor with *n*-type impurity conductivity at low temperatures and nearly intrinsic *p*-type conductivity at room temperature. Despite the severe disorder, the compound does not display low thermal conductivity and high thermoelectric figure-of-merit.

Acknowledgment. The authors acknowledge Dr. R. V. Shpanchenko for the high-accuracy X-ray powder data acquisition. A.V.O. thanks the Belgium Federal Science Policy office for research fellowship. E.V.D. is grateful to the National Science Foundation for funding the CCD diffractometer (CHE-0619422) at the University of Albany. This work is supported in part by Russian Foundation of Basic Research, Grants 06-03-32183 and 07-03-12155.

Supporting Information Available: Crystallographic information in CIF format. This material is available free of charge via the Internet at http://pubs.acs.org.

CM702655G